Dynamic Monte Carlo modeling of exciton dissociation in organic donor-acceptor solar cells

Michael C. Heiber and Ali Dhinojwala

Citation: J. Chem. Phys. **137**, 014903 (2012); doi: 10.1063/1.4731698
View online: http://dx.doi.org/10.1063/1.4731698
View Table of Contents: http://jcp.aip.org/resource/1/JCPSA6/v137/i1
Published by the American Institute of Physics.

Dynamic Monte Carlo modeling of exciton dissociation in organic donor-acceptor solar cells

Michael C. Heiber[a] and Ali Dhinojwala[b]
Department of Polymer Science, University of Akron, Akron, Ohio 44325, USA

(Received 20 January 2012; accepted 13 June 2012; published online 6 July 2012)

A general dynamic Monte Carlo model for exciton dissociation at a donor-acceptor interface that includes exciton delocalization and hot charge separation is developed to model the experimental behavior observed for the poly(3-hexylthiophene):fullerene system and predict the theoretical performance of future materials systems. The presence of delocalized excitons and the direct formation of separated charge pairs has been recently measured by transient photo-induced absorption experiments and has been proposed to facilitate charge separation. The excess energy of the exciton dissociation process has also been observed to have a strong correlation with the charge separation yield for a series of thiophene based polymer:fullerene systems, suggesting that a hot charge separation process is also occurring. Hot charge separation has been previously theorized as a cause for highly efficient charge separation. However, a detailed model for this process has not been implemented and tested. Here, both conceptual models are implemented into a dynamic Monte Carlo simulation and tested using a simple bilayer donor-acceptor system. We find that exciton delocalization can account for a significant reduction in geminate recombination when compared to the traditional, bound polaron pair model. In addition, the hot charge separation process could further reduce the geminate recombination, but only if the hot charge mobility is several orders of magnitude larger than the standard charge mobility. © *2012 American Institute of Physics*. [http://dx.doi.org/10.1063/1.4731698]

I. INTRODUCTION

Modeling and simulation of organic solar cells is important to test our understanding of the fundamental physics of device operation and allow us to make educated predictions for new devices. Many types of simulations ranging from numerical models[1,2] down to quantum level calculations[3] are being developed. Within this wide range of methods, dynamic Monte Carlo (DMC) simulations are unique in their ability to incorporate nanoscale details while maintaining the ability to simulate a complete device.[4] Retaining nanoscale detail is particularly important for modeling the complex morphologies present in bulk heterojunction solar cells.[5]

A DMC simulation of a full device is built by incorporating all dominant mechanisms involved in solar cell operation including exciton creation, exciton diffusion, exciton dissociation, exciton relaxation, charge transport, charge collection, charge injection, and charge recombination. Overall device performance is determined based on the rate of each competing mechanism and the accuracy of the final prediction is dependent on the quality of the model for each mechanism. One of the most difficult mechanisms to model has been exciton dissociation due to the complexity of the physical mechanisms involved.

Exciton dissociation is traditionally described as a two-step process. First, charge transfer takes place between the donor and the acceptor, causing a transition from an exciton state in one material to a polaron pair state (also called a geminate pair or charge transfer state) in which an electron and a hole are separated across the donor-acceptor interface. Second, the charges migrate away from each other to form free charge carriers. Normally, immediately after charge transfer, the distance between the two charges is assumed to be small enough that there would be a significant Coulomb attraction. Given a significant polaron pair binding energy, it would be expected that the pair would have a high probability of undergoing geminate recombination. However, highly efficient charge separation is observed for a range of optimized polymer:fullerene systems.

Understanding charge photogeneration at the donor-acceptor interfaces has been of great interest to both theoretical and experimental scientists studying organic solar cells. Several excellent reviews of the field have been recently published.[6,7] To explain the unexpectedly high geminate separation yield, several concepts have been proposed. However, additional simulation developments are needed to account for continuing experimental and theoretical progress. Understanding this fundamental aspect of solar cell operation is not only important for developing accurate simulations, but it is also particularly important for creating more efficient devices.

In the traditional, bound polaron pair model, a thermally activated separation process is required to overcome the polaron pair binding energy. However, the bound polaron pair state also has a characteristic lifetime which is used to determine the recombination rate. When the polaron pair binding energy is large, the charge separation yield is highly dependent on the recombination rate. Charge separation yield within this traditional model has also been shown to

[a]mch41@zips.uakron.edu.
[b]ali4@uakron.edu.

be promoted by energetic disorder[8–10] and mobility.[11,12] A full device DMC simulation built on this exciton dissociation model predicts relatively high geminate recombination losses. Even when using an optimized pillared morphology, geminate recombination of ∽35% is obtained using a recombination rate of 5×10^5 s^{-1}.[13] However, optimized polymer:fullerene systems have shown internal quantum efficiencies near 100% under short-circuit conditions, which suggests very little geminate recombination is occurring.[14–16]

In addition, transient photoinduced absorption experiments on the poly(3-hexylthiophene) (P3HT):phenyl-C61-butyric acid methyl ester (PCBM) system have measured a much higher recombination rate than typically used in the traditional, bound polaron pair model.[17,18] Simulating the geminate separation yield using this model with the experimentally determined recombination rates for the P3HT:PCBM system would be expected to lead to even higher geminate recombination. This traditional model has also been shown to be inadequate for describing the performance of small molecule organic solar cells.[19] While the traditional model described here has been successfully used to model the performance of some polymer-polymer devices, it has been unable to explain the high performance of polymer:fullerene and small molecule systems in previous studies.

In order to explain highly efficient charge separation, several additional theories have been proposed. Arkhipov *et al.* proposed that zero-point kinetic energy and interfacial dipoles reduce the geminate pair binding energy.[20,21] In addition, experimental evidence of the formation of interfacial dipoles through integer charge transfer has been provided by ultraviolet photoelectron spectroscopy studies.[22–24] However, an integer charge transfer model has not yet been incorporated into DMC device simulations.

A hot geminate pair dissociation concept has also been proposed by Peumans and Forrest.[25] This concept is derived from the hot exciton dissociation model used to explain photoconductivity behavior of bulk organic semiconductors.[26–28] A simple hot charge separation model has been used to predict the short-circuit current behavior of a range of organic solar cell device morphologies and can be fit to reproduce the low geminate recombination seen in experiments.[19] Experimental studies have also characterized the presence of hot charge transfer states in some donor-acceptor systems.[29,30] In addition, experiments on a range of thiophene based polymers mixed with fullerenes have shown a correlation between charge carrier generation and the magnitude of the excess energy of charge transfer.[31,32] Hot charge separation has also been proposed as an explanation for temperature independent charge separation.[33] On the other hand, several additional studies have indicated that hot charge separation may in fact not be significant.[34,35] In the first DMC model implementing this hot charge separation concept, Peumans and Forrest assume a simple linear relationship between the initial charge separation distance (thermalization distance) and the excess energy to illustrate the model.[25] However, a hot charge separation model based on a more complete physical picture has not been implemented.

Charge delocalization has also been proposed as a cause of efficient charge separation in polymer:fullerene systems by Deibel *et al.*[36] In this model, following charge transfer, the positive charge in the polymer donor is spread out along a polymer chain. By spreading the charge along the chain according to the conjugation length, the effective Coulomb attraction between the electron and hole is greatly reduced. This model is expected to be dependent on the chain configuration and orientation at the donor-acceptor interface. Chain configuration and orientation at the interface is largely unknown in most donor-acceptor systems and most DMC mechanisms have not yet been developed to incorporate charge delocalization and molecular details, which makes it difficult to implement this model into full device simulations at this time. However, Deibel *et al.* have shown that including charge delocalization can account for a significant decrease geminate recombination.[36]

In addition to charge delocalization, exciton delocalization has been measured to have significant effects on exciton behavior.[37] When excitons are very small, the majority of the excitons created in a bulk heterojunction device have to undergo diffusion until they reach an interface for dissociation. However, if excitons are delocalized over a larger space, a more significant fraction can dissociate immediately after creation. To quantify this behavior, Guo *et al.* have performed transient photoinduced absorption measurements on annealed bulk heterojunction regioregular P3HT:PCBM films which indicate that up to 50% of the excitons created in P3HT regions undergo immediate dissociation and the rest undergo diffusion prior to dissociating.[18] Guo *et al.* conclude that this behavior is consistent with their previous measurements of exciton delocalization where in regio-regular P3HT the delocalization radius is 4.3 nm in amorphous regions and 6.7 nm in core crystalline regions.[38] Marsh *et al.* have also observed similar behavior indicating significant exciton delocalization.[39]

Further results by Guo *et al.* show that free charges carriers are generated directly from excitons, suggesting that charge separation is not mediated by the formation of an intermediate charge transfer state. They propose that the initial separation distance between the charges is correlated with the exciton delocalization radius based on a comparison between regio-regular and regio-random P3HT.[18] This concept of exciton delocalization has not been implemented into DMC simulations and could help account for the low geminate recombination observed in optimized polymer:fullerene devices.

To advance this work, we start with a traditional, bound polaron pair DMC exciton dissociation model and implement a model for exciton delocalization and hot geminate pair separation. As a test case, all models are tested under simulated short-circuit conditions for a model donor-acceptor bilayer solar cell. As a point of reference, we first provide a brief assessment of the traditional exciton dissociation model by measuring the geminate recombination as a function of the recombination rate, energetic disorder and charge carrier mobility. We then implement the exciton delocalization model and measure the geminate recombination as a function of the magnitude of exciton delocalization. Finally, the hot charge separation model is included and the entire model tested using parameters similar to the P3HT:PCBM system. The final

model is then used to predict the dependence of geminate recombination on the donor-acceptor energy offset.

II. METHODOLOGY

A. Dynamic Monte Carlo method

The model bilayer device is constructed using a three-dimensional lattice with the top and bottom surfaces designated as the electrodes and periodic boundary conditions used for the side surfaces. The donor and acceptor materials are modeled as energetically disordered semiconductors with a Gaussian distribution of site energies.[40,41] The donor and the acceptor properties are assigned based on corresponding bulk properties. We assume a sharp interface and do not modify the properties near the interface in any way.

In recent studies on P3HT:PCBM blends, low energy states within the bandgap have been measured and are attributed to trap sites at or near the donor-acceptor interface.[42] While these interfacial trap sites have been linked to non-geminate recombination in P3HT:PCBM devices,[43–45] geminate recombination remains low despite the presence of interfacial trap sites,[46] suggesting that these trap sites have a limited effect on geminate recombination behavior. As a result, interfacial traps sites are not included in this study.

Also, we treat the energetic disorder of excitons separate from the energetic disorder of the charge transport energy levels to allow independent control of the energetic disorder parameters. The exciton energetic disorder, σ_{ex}, can be derived from singlet exciton absorption peak analysis[47,48] and the charge transport energetic disorder, σ_{ch}, can be derived from bulk charge transport modeling experiments.[49–52] In addition, the exciton energy level and the charge energy levels of each lattice site are assigned in correlated fashion, such that sites with a low exciton energy also have a low charge transport energy level and vice versa.

The simulation described here uses the first reaction method (FRM).[53] However, some modifications to the standard algorithm have been made. The DMC simulation employed here simulates all of the mechanisms relevant to exciton dissociation, including exciton creation, exciton hopping, exciton dissociation, exciton relaxation, charge hopping, charge collection, and charge recombination. In this study, charge injection is not included because injection current is negligible under short-circuit conditions. By using theoretical models for each of these mechanisms, the rate at which each of the events occur can be calculated. In the FRM, the wait time of each possible event is calculated and entered into a queue. Each event is assumed to be a first order process, and as a result, the wait time is calculated[53]

$$t = \frac{-\ln X}{R}, \tag{1}$$

where X is a random number between 0 and 1 chosen from a uniform distribution and R is the rate of the particular event. The event with the shortest wait time is then executed and the wait time of the executed event becomes the time step for the iteration. Following execution of each event, the queue is updated by adding or removing any newly enabled or disabled events, respectively.

Normally in the FRM, event wait times are calculated only once and remain in the queue until they are executed or become disabled. As a result, events in the queue are not modified when the conditions change. This has the potential to be a particularly significant issue for charges moving in an electrostatic landscape. Ideally, all events would be recalculated after each event is executed to make sure all changes are accounted for, but that method is computationally expensive. As a compromise, the model presented here uses a selective recalculation method. When a charge hops, nearby charges experience the strongest change in the Coulomb potential and will therefore be the most affected. As a result, when any charge hops, events are recalculated for all nearby charges within the cutoff distance of the initial and final sites. We find that this change introduces very little additional calculation time for the conditions tested here.

B. Exciton events

Exciton creation events are characterized by an exciton generation rate. The generation rate is determined by the light absorption properties of the donor and acceptor materials and is dependent on the device thickness as well as the intensity of the incident light. In real devices, the generation rate may be different at different regions of the active layer due to interference effects.[54] In this study, however, the exciton generation profile is assumed to be uniform. Also, in a real system, due to the wide absorption spectrum, excitons with a wide range of energies are created. However, hot excitons undergo extremely fast (<100 fs) vibrational relaxation,[38] and in this study, all excitons are assumed to undergo vibrational relaxation to the S_1 singlet state before other events occur. In addition, this study ignores the possible formation of triplet state excitons. The formation of triplet states is negligible in some materials and prevalent in others. For example, regioregular P3HT does not exhibit triplet formation, yet regiorandom P3HT exhibits significant conversion of singlet excitons to the triplet state.[38]

As a result, the exciton creation rate is calculated as

$$R_{exg} = GAd, \tag{2}$$

where G is the generation rate defined as excitons per unit volume per second, A is the area of the lattice, and d is the device thickness. When an exciton creation event is executed, the newly created exciton is assigned a random position within the lattice. Typical behavior of an exciton is that once created, it will hop randomly around in the material until it either relaxes back to the ground state or dissociates at the donor-acceptor interface. For a given material, the exciton relaxation time and the exciton diffusion length can be derived from transient photoluminescence quenching[55] and transient photoinduced absorption experiments.[17] The exciton relaxation time defines the lifetime of the excited state and is used to calculate the relaxation rate,

$$R_{exr} = 1/\tau_{ex}, \tag{3}$$

where τ_{ex} is the exciton lifetime. The exciton hopping rate is based on Förster energy transfer theory[56] as described

previously,[48]

$$R_{exh,ij} = R_{0,exh}\left(\frac{a}{d_{ij}}\right)^6 f_1(\Delta E_{ij,exh}), \tag{4}$$

where $R_{0,exh}$ is the exciton hopping coefficient, a is the lattice spacing size, d_{ij} is the distance between sites, and $\Delta E_{ij,exh}$ is the change in potential energy for exciton hopping,

$$\Delta E_{ij,exh} = E_{singlet,j} - E_{singlet,i}. \tag{5}$$

Here, $f_1(\Delta E_{ij})$ is the generic function which determines whether or not the Boltzmann factor is included in the rate equation

$$f_1(\Delta E_{ij}) = \begin{cases} \exp\left(\frac{-\Delta E_{ij}}{kT}\right) & \Delta E_{ij} > 0 \\ 1 & \Delta E_{ij} \leq 0 \end{cases}. \tag{6}$$

Exciton hopping is not restricted to nearest neighbor sites, and excitons have a small probability of hopping to more distant sites. However, because $R_{exh} \propto (1/d)^6$, short hops are highly favored and hopping events are only calculated for destination sites within a three lattice spacing radius. The exciton hopping coefficient is used as a fitting parameter and can be adjusted along with the exciton lifetime, until the simulated average diffusion length of the excitons in the lattice equals the diffusion length desired. Here, given an exciton lifetime of 330 ps in P3HT (Ref. 38) and an assigned hopping speed of 3×10^{12} s^{-1}, an average diffusion length of 17 nm of simulated. While this value is slightly larger than measured experimentally, the geminate recombination is not significantly affected by the magnitude of the exciton diffusion length. A larger diffusion length is implemented to decrease the computation time for the bilayer morphology.

As an exciton approaches the donor-acceptor interface, exciton dissociation becomes an enabled process. The first step in exciton dissociation, charge transfer, is calculated based on Miller-Abrahams theory,[57]

$$R_{exd} = R_{0,exd}\exp(-2\gamma_{ex}d_{ij})f_1(\Delta E_{ij,exd}), \tag{7}$$

where R_{exd} is the exciton dissociation coefficient, γ_{ex} is the inverse exciton localization parameter, $f_1(\Delta E_{ij,exd})$ is a function defined in Eq. (6), and $\Delta E_{ij,exd}$ is the change in potential energy for the charge transfer step of exciton dissociation. Here, the inverse exciton localization parameter is a material property which is used here to describe the amount of exciton delocalization. As the inverse exciton localization decreases, excitons effectively become more delocalized and the probability of dissociating when further away from the interface increases. The exciton dissociation coefficient is set to 10^{15} s^{-1} in this simulation so that exciton dissociation is a highly favorable event and is a diffusion limited process. For an exciton initially located in the donor material, the energy change of the charge transfer process is calculated

$$\Delta E_{ij,exd} = E_{\mathrm{HOMO}_D,i} - E_{\mathrm{LUMO}_A,j} - E_{singlet,i} + E_B - E_{GP}(d_{ij}) + Fd_z, \tag{8}$$

where E_B is the exciton binding energy, $E_{GP}(d_{ij})$ is the geminate pair binding energy, which is a function of the distance between sites, F is the electric field, and d_z is the z-component of the distance between sites. An analogous expression is used to calculate the energy change for excitons dissociating from the acceptor material. The geminate pair binding energy is the Coulomb potential between the two charges immediately after charge transfer

$$E_{GP}(d_{ij}) = \frac{e^2}{4\pi\epsilon\epsilon_0 d_{ij}}, \tag{9}$$

where e is the elementary charge, ϵ is the dielectric constant, and ϵ_0 is the vacuum permittivity constant. The dielectric constant used in previous simulation studies has ranged from 3.5 to 4.0. Here, we use a value of 3.8 as an intermediate magnitude that approximates many organic semiconducting materials.

In addition, for a large LUMO_D-LUMO_A and HOMO_D-HOMO_A offset energy, the charge transfer process will be exothermic, resulting in a negative energy change. In the hot dissociation model presented here, this excess energy creates a hot electron and a hot hole each with vibrational energy equal to half of the excess energy. Similar to previous work describing hot exciton dissociation in bulk semiconducting polymers, this extra vibrational energy increases the effective local temperature and contributes to thermally activated charge separation.[26,27] Competing with this thermally activated charge separation is a cooling process through which the local temperature eventually reaches ambient temperature. All other possible exciton events, including exciton-exciton annihilation, bulk exciton dissociation, and exciton-charge interactions are disregarded because their occurrence is negligible with the low concentration of excitons and charges under the conditions tested here.

C. Charge events

Charge transport in this model is based on Miller-Abrahams theory[57] in the same way as the charge transfer step for exciton dissociation. For electron hopping

$$R_{elh} = \alpha R_{0,elh}\exp(-2\gamma_{ch}d_{ij})f_2(\Delta E_{ij,elh}), \tag{10}$$

where α is the hot hopping enhancement factor, $R_{0,elh}$ is the electron hopping coefficient, γ_{ch} is the inverse charge delocalization parameter, and $f_2(\Delta E_{ij,elh}, E_v)$ is a modified Boltzmann function which accounts for the excess vibrational energy, E_v,[26]

$$f_2(\Delta E_{ij}) = \begin{cases} \exp\left(\frac{-\Delta E_{ij}}{kT+E_v}\right) & \Delta E_{ij} > 0 \\ 1 & \Delta E_{ij} \leq 0 \end{cases}. \tag{11}$$

The hot hopping enhancement factor is a constant value when the excess vibrational energy is greater than zero, and equal to one when the excess vibrational energy is equal to zero. An analogous expression is used to calculate hole hopping. As a further restriction, electron hopping is limited to only acceptor sites, and hole hopping is limited to donor sites. Similar to exciton hopping, hopping events are calculated for sites up to three lattice spacings away. The change in energy for an electron hopping event is calculated

$$\Delta E_{ij,elh} = E_{\mathrm{LUMO},i} - E_{\mathrm{LUMO},j} + \Delta E_{C,ij} - Fd_{ij}, \tag{12}$$

where $\Delta E_{C,ij}$ is the change in Coulomb potential that would occur for hopping from site i to site j.

Based on this treatment, when the vibrational energy is large, $f_2(\Delta E_{ij,elh})$ approaches unity. As a result, there is no preference between upward energy hops and downward energy hops. However, in this model, the vibrational energy also dissipates over time. Here we simulate this energy dissipation process as a series of ten stochastic relaxation events. The rate of each cooling event is calculated

$$R_{cool} = \beta / \Delta E_v, \tag{13}$$

where β is the cooling rate constant and ΔE_v is 1/10 of the initial vibrational energy of the charge. Cooling events continue until the vibrational energy reaches zero. Cooling is split up into 10 steps because every process must have discrete events in a DMC simulation. By using a constant cooling rate, a linear cooling process is simulated, similar to the work of Arkhipov *et al.*[26] This linear cooling process is further approximated by a step function due to the time interval between cooling events. A large number of steps would be used to most accurately simulate a gradual linear cooling process, but would introduce additional calculation time. If too few steps are used, the approximation of the linear cooling process is very poor. To ensure that enough steps are being used, we have also tested the system using 15 and 20 steps for a high starting vibrational energy, but no significant change in geminate recombination is observed. An exponential cooling process has also been used by Arkipov *et al.* in a later study to approximate the vibrational relaxation process,[27] but is not implemented here. In absence of more specific knowledge of how the vibrational state of a hot charge carrier relaxes over time, a simple linear cooling process is used to approximate what is likely a much more complex process.

Coulomb interactions between charges are important calculations that can have a strong impact on charge recombination behavior, but can also be computationally intensive. To save computation time, Coulomb interactions are only calculated for charges within a certain distance of each other. This distance is called the cutoff distance, r_{cut}, and it has been shown that when the cutoff distance is set to the thermal capture radius, the difference between a full Coulomb calculation and the cutoff method is minimal at short-circuit conditions.[58] In this study, with a dielectric constant of 3.8, the thermal capture radius is $\backsim$15 nm, so the cutoff distance is set to this value. Sample tests were also performed for larger cutoff radii of 17 nm and 19 nm and for the low charge density cases simulated here, no significant change in geminate recombination was observed. The change in Coulomb potential for an electron is calculated

$$\Delta E_{C,ij} = E_{C,j} - E_{C,i}, \tag{14}$$

where

$$E_{C,i} = \sum_{k=1,k\neq i}^{N} \frac{q_i q_k}{4\pi\epsilon\epsilon_0 d_{ik}} \qquad d_{ik} \leq 15 \text{ nm}, \tag{15}$$

given N electrons and holes. An analogous expression is used to calculate the Coulomb potential for the final state by assuming that the charge of interest is positioned on site j. In addition, when the charge is near an electrode, the Coulomb potential is further modified by the image charge attraction. Also, when a charge is close to an electrode, the charge collection event is enabled. The rate of charge collection is calculated in the exact same manner as charge hopping.

The electron hopping coefficient, $R_{0,\,elh}$, can be expressed as a function of the mobility as shown by Watkins *et al.*,[5]

$$R_{0,elh} = \frac{6kT\mu_{in}}{ea^2} \exp(2\gamma_{ch}a), \tag{16}$$

where μ_{in} is the input mobility. However, it is important to note that this derivation assumes isoenergetic hopping sites. Because an energetically disordered system is used here, it is questionable whether this simplified relationship results in accurate charge transport behavior. In particular, it has been shown that energetic disorder causes a reduction in the average mobility and an increase in dispersion.[41]

To resolve this issue, the effective mobility is determined for a range of input mobility and energetic disorder values using a separate DMC test. In this test, a $100 \times 100 \times 100$ lattice is created to represent a section of one material. Charges are placed one at a time at a random position along the top surface of the lattice and are then allowed to undergo normal hopping behavior. When a charge reaches the bottom surface, the transit time is recorded. Transit time data are collected for 5000 charges and a resulting average effective mobility then calculated. By recording data for one charge at a time, the effective mobility measured represents the behavior expected at a low charge density, which is in the same regime that most organic solar cells operate. The dependence of the effective mobility on the input mobility and energetic disorder is shown in the supplementary material.[59]

When an electron and a hole come close together, the charge recombination event is enabled. In this study, charge recombination is treated similar to charge hopping

$$R_{rec} = R_{0,rec} \exp(-2\gamma_{ch} d_{ij}), \tag{17}$$

where $R_{0,\,rec}$ is a fitting parameter which is tuned to obtain a particular recombination rate. The Boltzmann function is not included because charge recombination is an energetically favorable process. To provide a convenient comparison to previous experimental and modeling studies, we also define the characteristic recombination rate to be the magnitude of R_{rec} when the electron and hole are on adjacent sites

$$R_{crec} = R_{0,rec} \exp(-2\gamma_{ch} a). \tag{18}$$

D. Performance measurement

The main metric that will be used to gauge the performance of each model is the geminate recombination. To simplify this investigation, we will focus on the behavior at typical short-circuit conditions. Experimental quantum efficiency measurements are also performed under short-circuit conditions, which provides a frame of reference for this study. Typically, the internal electric field is $\backsim 10^6$ to 10^7 V/m at short-circuit. For a donor-acceptor bilayer with semiconducting polymers that have low charge carrier concentrations, the

donor and acceptor regions become completely depleted, and a uniform electric field is formed across the device thickness. As a result, in this study, the electric field will be set to 10^7 V/m across the entire device thickness.

When calculating the geminate recombination, each test was run until 1000 excitons had been dissociated. To quantify the recombination behavior, electrons and holes are tagged as they are created in order to allow a distinction between geminate recombination and bimolecular recombination. However, for a bilayer device under the conditions tested here, bimolecular recombination was negligible. To reduce energetic configuration bias, each test was performed N times and the final measurements were obtained by determining the average and standard deviation of the set of measurements. The traditional model was tested for N = 10, but very little variation was seen between each test. In subsequent tests, each condition was only tested 5 times (N = 5) to save computation time.

To determine effective exciton interaction radius separate tests were performed. In this test, the creation of excitons is restricted to sites away from the interface. The minimum distance allowed was set to larger than the tail of the interaction radius distribution to make sure that excitons would undergo some diffusion prior to dissociation. The test was run until 1000 excitons had been dissociated. After each exciton dissociation event, the distance between the exciton and the interface is recorded. The collected data form a Gaussian distribution which describes the interaction radius for the given set on input parameters. The average and standard deviation of this distribution is used to characterize the effective exciton interaction radius.

The choice of all input parameters has been done to closely reflect real materials and is largely based on the regioregular P3HT system. As a donor material, P3HT has an optical bandgap of about 1.9 eV and a transport gap of 2.6 eV, resulting in an exciton binding energy of $\backsim$0.7 eV.[60] The acceptor material is assumed to be identical to P3HT in all ways except for the relative position of the HOMO and LUMO energy levels. An exciton generation rate of 10 nm^{-3} s^{-1} is used as an approximate magnitude for P3HT:PCBM blends at 1 sun intensity, which corresponds to a short circuit current of about 16 mA/cm^{-2} when assuming all excitons are extracted as current. In a real system, such as P3HT:PCBM, PCBM has slightly different properties, such as a lower exciton generation rate, a higher mobility, and a longer exciton diffusion length than P3HT. However, charge generation in P3HT:PCBM has been shown to be dominated by excitons formed in the P3HT regions. Tests have been performed where excitons are formed in both the donor and the acceptor and where they are only allowed to be formed in the donor. This change affects the magnitude of photocurrent, but does not affect the geminate recombination behavior.

To simplify the system in this study, we also assume that the energetic disorder of the excitons and charges are equal and that both the donor and acceptor have equivalent energetic disorder. While this is not true for all materials and the exciton energetic disorder is often larger than the charge transport energetic disorder,[61] the magnitudes are approximately equal for P3HT.[50,60] A complete list of simulation parameters is shown in Table I.

TABLE I. Simulation parameters.

Donor thickness	20 nm
Acceptor thickness	20 nm
Lattice spacing, a	1 nm
Lattice length	50 sites
Lattice width	50 sites
Lattice height	40 sites
Exciton generation, G	10 nm^{-3} s^{-1}
Temperature, T	300 K
Exciton lifetime, τ_{ex}	330 ps
Exciton hopping rate constant, $R_{0,exh}$	3×10^{12} s^{-1}
Exciton dissociation rate constant, $R_{0,exd}$	10^{15} s^{-1}
Charge recombination rate constant, $R_{0,rec}$	10^{11} s^{-1}
Exciton binding energy, E_B	0.7 eV
Inverse charge delocalization, γ_{ch}	2 nm^{-1}
Dielectric constant, ϵ	3.8
Cutoff distance, r_{cut}	15 nm

To study the effect of the excess energy on the hot geminate pair dissociation model, we also need to be able to control the excess energy of the charge transfer process. From Eq. (8), we find that the excess energy of the initial charge transfer step is governed mainly by the magnitude of the energy level change when an electron hops from the LUMO of the donor to the LUMO of the acceptor. For an exciton created in the acceptor, where there is hole transfer from the acceptor to the donor, the $HOMO_D$-$HOMO_A$ energy level offset is the important feature. In this study, the bandgap of the donor and the acceptor are equal, resulting in equal $LUMO_D$-$LUMO_A$ and $HOMO_D$-$HOMO_A$ offset energies. These offset energies can then be generalized as the donor-acceptor energy offset, ΔE_{DA}. To control the magnitude of the excess energy of the charge transfer process, the simulation was run for several different magnitudes of donor-acceptor energy offset, keeping the exciton binding energy as a constant.

III. RESULTS AND DISCUSSION

A. Traditional geminate pair dissociation

In pursuit of an exciton dissociation model that can explain the high performance seen in optimized polymer:fullerene systems, the traditional model is characterized first. In order to reach experimental internal quantum efficiencies observed for optimized polymer:fullerene systems, the geminate recombination must be less than 10%. As discussed previously, geminate separation yield in this model is aided by having a low recombination rate, high mobility, and high energetic disorder. Transient photoinduced absorption studies on P3HT:PCBM blends have resulted in recombination rate measurements several orders of magnitude larger than often used in traditional exciton dissociation simulations. To quantify the effect of the recombination rate independently, approximate values for the mobility and the energetic disorder of P3HT were used. Figure 1 shows the geminate separation yield results for a system with an effective mobility of 5×10^{-4} $cm^2/(Vs)$ and an energetic disorder of 0.07 eV.

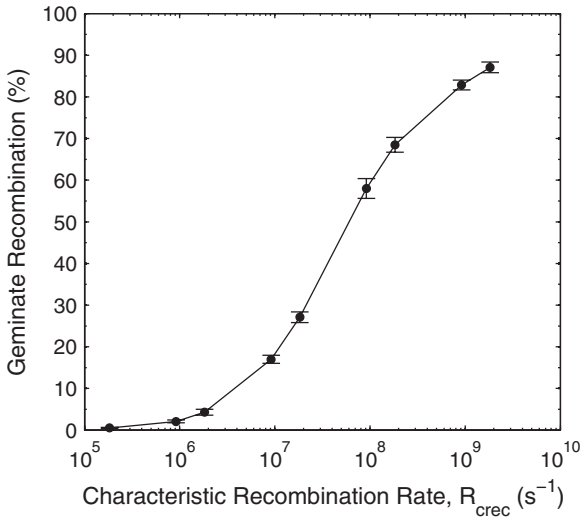

FIG. 1. Geminate recombination vs. characteristic recombination rate, R_{crec}, for $\mu_{eff} = 5 \times 10^{-4}$ cm^2/(Vs) and $\sigma = 0.07$ eV.

For recombination rates of 10^5 and 10^6 s^{-1}, low geminate recombination is reached, yet for larger recombination rates in the range of 10^8 and 10^9 s^{-1}, extremely high geminate recombination is observed. For the P3HT:PCBM system, the recombination rate has been determined to be on the order of 10^9 s^{-1}.[17,18]

It is possible that this model may still work with a higher recombination rate if the disorder and/or mobility are greater than assumed previously. Here, we fix the recombination rate at 10^9 s^{-1} and gather geminate recombination statistics using the traditional dissociation model for a range of different magnitudes of effective mobility and energetic disorder. The effective mobility is a measured parameter in the system, which is controlled by adjusting the charge hopping speed for a given value of energetic disorder as described in more detail in Sec. II. Figure 2 shows the geminate recombination as a function of the average effective mobility for four different magnitudes of energetic disorder, 0.05, 0.075, 0.1, and 0.125 eV. Here, energetic disorder has a strong effect on the geminate recombination. For a constant effective mobility of 10^{-5} cm^2/(Vs), the geminate recombination decreases from almost 100% at 0.05 eV energetic disorder down to about 20% at 0.125 eV energetic disorder. However, the traditional model is still unable to produce geminate recombination values less than 10% for the conditions tested here and will only reach such a low magnitude when both the mobility and energetic disorder are high.

Materials with higher energetic disorder in the range shown do exist, but these materials often have relatively low mobility. Most materials would not be expected to have both high mobility and high energetic disorder. For example, P3HT has an energetic disorder of about 0.07 eV, based on charge transport modeling experiments,[50] and a bulk mobility in the range of 10^{-4} to 10^{-3} cm^2/(Vs) based on time of flight measurements.[50,62] In general, disorder is expected to reduce mobility, so it is unusual to have both high mobility and high disorder. Other semiconducting polymers with larger energetic disorder of around 0.1 eV have mobilities which are several orders of magnitude lower than P3HT.[63] In addition, the thermally activated separation process in the traditional model is expected to be highly temperature dependent, yet experimental results indicate that free carrier generation in polymer:fullerene devices is temperature independent.[33,64] These results agree with previous studies which have shown that the traditional, bound polaron pair model inadequately describes the behavior observed for polymer:fullerene devices.

B. Exciton delocalization

The first addition to the traditional model discussed here is exciton delocalization. As described earlier, exciton delocalization is inferred from experimental measurements of the exciton interaction radius. The main parameter controlling the interaction radius in this model is the inverse exciton

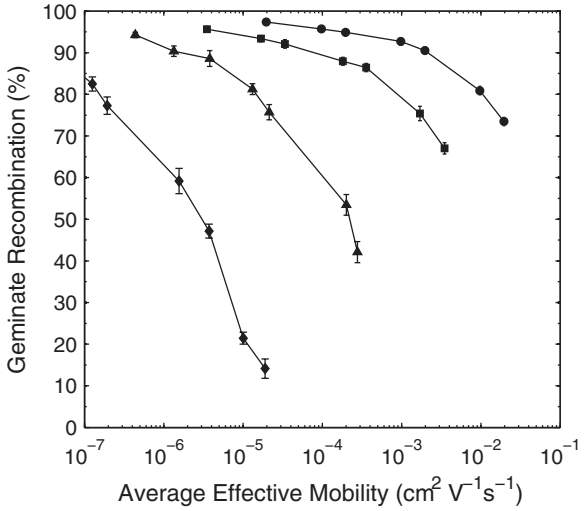

FIG. 2. Geminate recombination vs. average effective mobility for several magnitudes of energetic disorder, $\sigma = 0.05$ eV (circles), $\sigma = 0.075$ eV (squares), $\sigma = 0.1$ eV (triangles), and $\sigma = 0.125$ eV (diamonds).

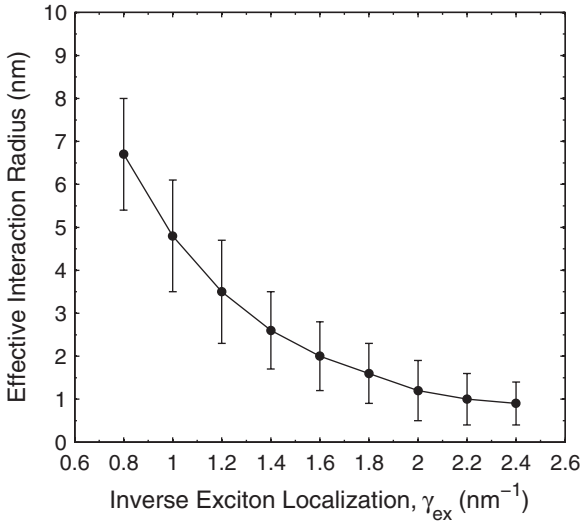

FIG. 3. Effective interaction radius vs. inverse exciton localization for $\mu_{eff} = 5 \times 10^{-4}$ cm^2/(Vs) and $\sigma = 0.07$ eV.

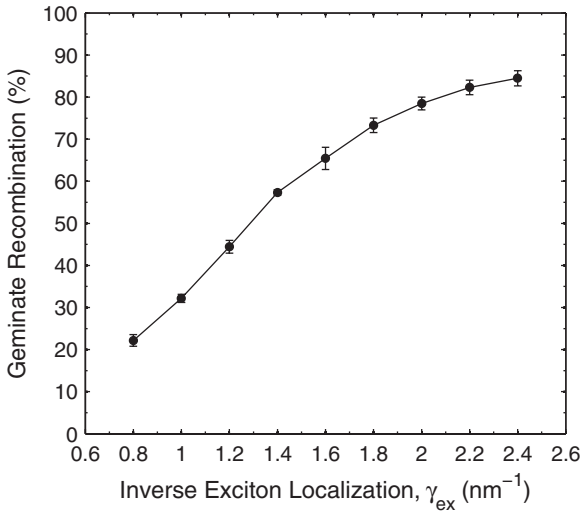

FIG. 4. Geminate recombination vs. inverse exciton localization for $\mu_{eff} = 5 \times 10^{-4}$ cm^2/(Vs) and $\sigma = 0.07$ eV.

localization parameter, γ_{ex}. Figure 3 shows how the effective interaction radius depends on the magnitude of the inverse exciton localization parameter. Here, the error bars represent the standard deviation of the interaction radius distribution. The distribution also becomes broader as the interaction radius increases.

The result of exciton delocalization in this model is that charges are initially separated by a larger distance following charge transfer. This behavior is very similar to that obtained by Deibel *et al.* using their charge delocalization model.[6] In their charge delocalization model, spreading of partial charges along the polymer chain results in an larger effective separation distance between the electron and the hole. This larger separation distance results in a weaker Coulomb attraction and thus a higher probability of separation. In Figure 4, geminate recombination shows a strong dependence on delocalization going from about 90% geminate recombination for localized excitons in the traditional model down to about 20% when the interaction radius reaches about 7 nm.

As discussed previously, the interaction radius for regioregular P3HT has been experimentally determined to be between 4.3 and 6.7 nm depending on whether the excitons are in the amorphous or crystalline regions, respectively.[18] Here, we assume a more simplified system with homogenous behavior such that all excitons created in the material have the same amount of delocalization. For further simulations, the inverse delocalization was set to 1.0 nm^{-1}. At this condition, the interaction radius is 4.8 ± 1.3 nm and the geminate recombination is about 32%. It is important to note that this model predicts that geminate recombination is strongly dependent on the magnitude of delocalization. Given that very few experimental studies have been done to characterize the interaction radius of delocalized excitons, further investigation of this parameter is of particular interest. While 32% geminate recombination is a significant improvement from the traditional model, additional refinements are needed to reach the target of 10%.

C. Hot geminate pair dissociation

In an attempt to further reduce the geminate recombination and model the excess energy dependence of free carrier generation, a hot geminate pair dissociation model is proposed. The hot exciton dissociation model constructed by Arkhipov *et al.* and the model implemented here both present a competition between the hopping speed of hot charges and the cooling process.[26,27] Looking back at the Boltzmann function used for charge hopping in Eq. (11), when the vibrational energy is large, the exponential term approaches unity and charge hopping becomes independent of the Coulomb interactions between charges. As a result, hot charge hopping behaves like a random walk until the vibrational energy dissipates. The distance between the electron and the hole once both charges cool back down to ambient temperature depends on both the hopping rate and the lifetime of the hot state. Depending on the initial vibrational energy and the cooling rate, each system will have different effective lifetimes for hot charge hopping. Depending on the charge carrier mobility and the hot hopping enhancement factor, each system will have a different hopping speed.

To characterize these competing factors, we keep the effective mobility constant, and test the behavior for several magnitudes of hot hopping enhancement factor, α, and the cooling rate, β. For the system simulated here, ΔE_{DA} is set to 2.0 eV based approximately on the LUMO$_D$-LUMO$_A$ offset determined experimentally for P3HT and PCBM. The exact magnitude of the LUMO$_D$-LUMO$_A$ offset is hard to conclude due to the large variation of values reported for the HOMO and LUMO energy levels of organic semiconductors depending on which experimental techniques are used and the quality of the sample. Here we rely on ultraviolet photoelectron spectroscopy and inverse photoelectron spectroscopy studies on bulk materials to provide the best estimate of the transport energy levels for P3HT and PCBM. Based on a measurement of 4.5 eV for the hole transport level of annealed regioregular P3HT (Ref. 24) and a transport gap of 2.6 eV,[60] the electron transport level of P3HT is estimated to be 1.9 eV. PCBM has also been characterized to have an electron transport level at 3.9 eV,[65] suggesting a LUMO$_D$-LUMO$_A$ offset of up to 2.0 eV in the P3HT:PCBM system. However, slightly lower values have also been estimated in previous studies.[31] The HOMO$_D$-HOMO$_A$ offset of the P3HT:PCBM is disregarded because the performance of the P3HT:PCBM system has been shown to be dominated by excitons formed in P3HT which depend on the LUMO$_D$-LUMO$_A$ offset for dissociation.

Figure 5 shows how geminate recombination is affected by the normalized cooling rate for this system. Here we find that when normalizing the cooling rate by the hot hopping enhancement factor, all datasets tested fall onto roughly the same curve. To ensure that the results are not affected by the lattice dimensions, tests in this regime were also done on a system with a 60 nm thickness and no significant differences were observed. From this analysis, we find that the geminate recombination reaches less than 10% when the normalized cooling rate is less than 1×10^9 eV/s. Relaxation of vibrational energy is typically thought to be a very fast process on a timescale of roughly 100 fs. In the original work by

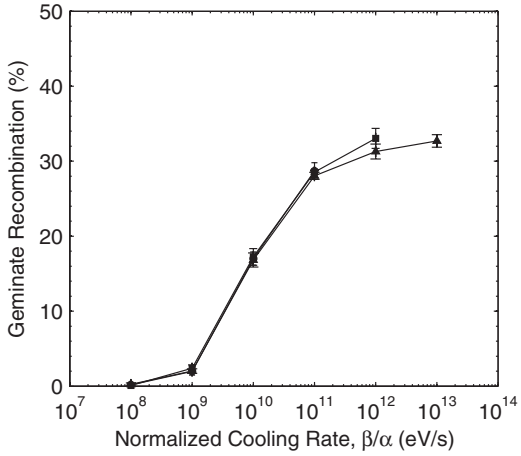

FIG. 5. Geminate recombination vs. normalized cooling rate for $\Delta E_{DA} = 2.0$ eV, $\mu_{eff} = 5 \times 10^{-4}$ cm^2/(Vs), $\sigma = 0.07$ eV, $\beta = 1 \times 10^{11}$ eV/s (circles), $\beta = 1 \times 10^{12}$ eV/s (squares), $\beta = 1 \times 10^{13}$ eV/s (triangles).

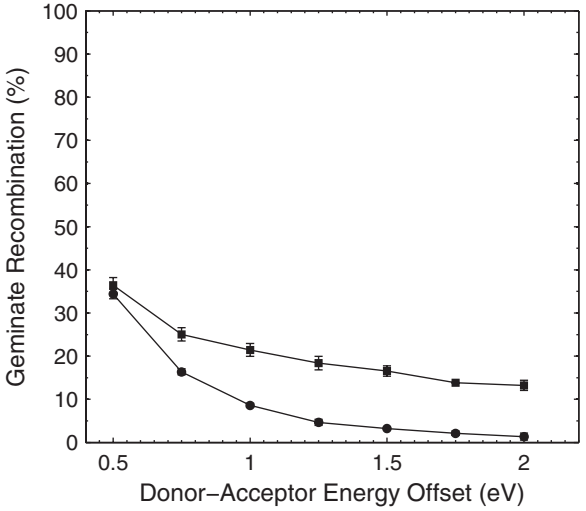

FIG. 6. Geminate recombination vs. donor-acceptor energy offset for $\mu_{eff} = 5 \times 10^{-4}$ cm^2/(Vs), $\sigma = 0.07$ eV, $\gamma_{ex} = 1.0$ nm^{-1}, $\beta = 1 \times 10^{12}$ eV/s, $\alpha = 1000$ (circles), $\alpha = 100$ (squares).

Arkipov *et al.*, a cooling rate of 10^{12} eV/s is used to describe the vibrational relaxation of hot excitons.[26] For the model tested here, given a cooling rate of 10^{12} eV/s, a hot hopping enhancement factor of 1000 is needed to reach a geminate recombination of less than 10%. In addition, when the hot hopping enhancement factor is set to 1, almost no reduction in geminate recombination is observed. As a result, if the hopping speed of hot charges is equal to that of cold charges, the vibrational energy dissipates too fast to significantly contribute to charge separation. It may be possible that hot charges hop at a faster rate than normal. However, to the authors' knowledge, hot charge mobility in organic semiconductors has not been studied. We find that for hot charge hopping separation to have a significant effect on the geminate recombination, either hot charge mobility must be at least two to three orders of magnitude larger than the typical bulk mobility or the vibrational relaxation rate must be significantly slower than expected. To predict the excess energy dependence of charge separation in further tests, we assume that the cooling rate is 10^{12} eV/s and that the hot charge hopping is fast by adjusting the hot hopping enhancement factor.

At this point, the complete model has been fit to simulate a system with delocalized excitons and a very large donor-acceptor energy offset. However, the dependence of the geminate recombination on the donor-acceptor energy offset is of particular importance for developing new materials and improved devices. Figure 6 shows this relationship for several cooling rates, keeping all other parameters constant. This model predicts that the geminate recombination has a weak dependence on ΔE_{DA} when ΔE_{DA} is large. However, when ΔE_{DA} is less than 1.0 eV , the geminate recombination starts to increase significantly. Below $\Delta E_{DA} = 0.6$ eV, exciton dissociation starts to decrease due to a negative excess energy, so we focus here on the regime where exciton dissociation is constant. When decreasing the hot hopping enhancement factor, the correlation is even weaker and the overall magnitude of geminate recombination increases.

The weak dependence observed here is unexpected and is partly caused by the large initial separation distance due to exciton delocalization. Figure 7 shows the behavior of the system when the exciton delocalization is decreased. Here, $\gamma_{ex} = 2.2$ nm^{-1}, leading to an average interaction radius of about 1 nm. In this case, the geminate recombination increases much more when the donor-acceptor offset energy is low. However, the dependence still remains weak in the regime near the P3HT:PCBM system.

In all cases, however, the relatively weak dependence of geminate recombination on ΔE_{DA} in this regime is unexpected based on experimental measurements which have indicated a much stronger effect. Ohkita *et al.* have measured charge generation on a group of thiophene based polymers with different energy levels, and for the semi-crystalline polymers tested, the charge carrier generation was observed to decrease by two orders of magnitude when lowering the excess energy by only 0.3 eV.[31] Conversely, Rand *et al.* have modeled experimental results for a series of small molecule

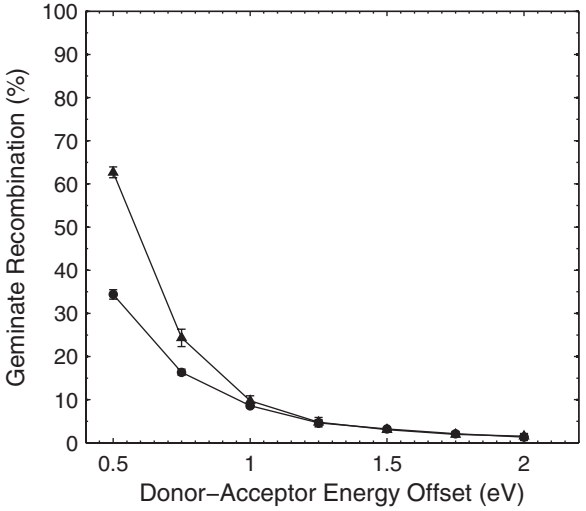

FIG. 7. Geminate recombination vs. donor-acceptor energy offset for $\mu_{eff} = 5 \times 10^{-4}$ cm^2/(Vs), $\sigma = 0.07$ eV, $\alpha = 1000$, $\beta = 1 \times 10^{12}$ eV/s, $\gamma_{ex} = 1.0$ nm^{-1} (circles), and $\gamma_{ex} = 2.2$ nm^{-1} (triangles).

donor-acceptor bilayer devices and predict a similarly weak dependence on ΔE_{DA}.[66] Rand *et al.* show a weak change in short-circuit current as a function of ΔE_{DA} in the regime where ΔE_{DA} is large, which is consistent with the results obtained here.

In simulations it is easy to control the system so that there is only one independent variable, but in experiments each material tested may have a different recombination rate, carrier mobility, exciton binding energy, or exciton delocalization, which could lead to ambiguous results. While the materials tested by Ohkita *et al.* were all semi-crystalline polymers and may be expected to have similar exciton delocalization behavior, direct measurements are needed to characterize each material in more detail. Since very few materials systems are as well characterized as P3HT:PCBM at this time, it is difficult to know whether the experimentally observed trend is an accurate representation of general behavior. At this time, additional experiments need to be performed in order to confirm the hot dissociation model presented here.

IV. CONCLUSIONS

In agreement with previous studies, the traditional, bound polaron pair model cannot reproduce the low geminate recombination seen in optimized polymer:fullerene devices. In working towards a more complete exciton dissociation model, an exciton delocalization model and a hot charge separation model were implemented. Within these models, a significant decrease in geminate recombination is observed as the exciton interaction radius increases and the normalized cooling rate decreases. Our analysis of the hot charge separation model reveals that the hot charges must hop 100–1000 times faster than cold charges, otherwise the excess vibrational energy is likely to dissipate too fast to significantly contribute to charge separation. Under this assumption, together these models are able to reproduce the low geminate recombination observed in optimized polymer:fullerene systems using input parameters typical for the regioregular P3HT:PCBM system.

Further investigation of the dependence of the geminate recombination on the donor-acceptor energy offset reveals a relatively weak relationship in the regime near the P3HT:PCBM system, where ΔE_{DA} is around 2.0 eV. Experimental verification of this trend is currently inconclusive and additional experimental studies investigating the effects of the donor-acceptor energy offset on device performance are needed. By expanding this new exciton dissociation model to a full device simulation, a more accurate description of organic solar cells may be possible.

ACKNOWLEDGMENTS

We thank the LORD Corporation and the National Science Foundation Grant Nos. NSF-DMR 0512156 and NSF-DMR 1105370 for funding and Professor Mesfin Tsige for discussions and simulation help. We also thank the Southern Illinois University SIHPCI for computation time.

[1] J. A. Barker, C. M. Ramsdale, and N. C. Greenham, Phys. Rev. B **67**, 075205 (2003).
[2] L. J. A. Koster, E. C. P. Smits, V. D. Mihailetchi, and P. W. M. Blom, Phys. Rev. B **72**, 085205 (2005).
[3] V. Lemaur, M. Steel, D. Beljonne, J.-L. Brédas, and J. Cornil, J. Am. Chem. Soc. **127**, 6077 (2005).
[4] L. Meng, Y. Shang, Q. Li, Y. Li, X. Zhan, Z. Shuai, R. G. E. Kimber, and A. B. Walker, J. Phys. Chem. B **114**, 36 (2010).
[5] P. K. Watkins, A. B. Walker, and G. L. B. Verschoor, Nano Lett. **5**, 1814 (2005).
[6] C. Deibel, T. Strobel, and V. Dyakonov, Adv. Mater. **22**, 4097 (2010).
[7] T. M. Clarke and J. R. Durrant, Chem. Rev. **110**, 6736 (2010).
[8] U. Albrecht and H. Bässler, Chem. Phys. Lett. **235**, 389 (1995).
[9] S. Barth, D. Hertel, Y.-H. Tak, H. Bässler, and H. H. Hörhold, Chem. Phys. Lett. **274**, 165 (1997).
[10] T. Offermans, S. C. J. Meskers, and R. A. J. Janssen, Chem. Phys. **308**, 125 (2005).
[11] C. Groves, R. A. Marsh, and N. C. Greenham, J. Chem. Phys. **129**, 114903 (2008).
[12] M. Wojcik, P. Michalak, and M. Tachiya, Appl. Phys. Lett. **96**, 162102 (2010).
[13] R. A. Marsh, C. Groves, and N. C. Greenham, J. Appl. Phys. **101**, 083509 (2007).
[14] S. H. Park, A. Roy, S. Beaupré, S. Cho, N. Coates, J. S. Moon, D. Moses, M. Leclerc, K. Lee, and A. J. Heeger, Nat. Photonics **3**, 297 (2009).
[15] H.-Y. Chen, J. Hou, S. Zhang, Y. Liang, G. Yang, Y. Yang, L. Yu, Y. Wu, and G. Li, Nat. Photonics **3**, 649 (2009).
[16] Y. Liang, J. Xia, S.-T. Tsai, Y. Wu, G. Li, C. Ray, and L. Yu, Adv. Mater. **22**, E135 (2010).
[17] I.-W. Hwang, D. Moses, and A. J. Heeger, J. Phys. Chem. C **112**, 4350 (2008).
[18] J. Guo, H. Ohkita, H. Benten, and S. Ito, J. Am. Chem. Soc. **132**, 6154 (2010).
[19] F. Yang and S. R. Forrest, ACS Nano **2**, 1022 (2008).
[20] V. I. Arkhipov, E. V. Emelianova, and H. Bässler, Chem. Phys. Lett. **372**, 886 (2003).
[21] V. I. Arkhipov, P. Heremans, and H. Bässler, Appl. Phys. Lett. **82**, 4605 (2003).
[22] Z. Xu, L.-M. Chen, M.-H. Chen, G. Li, and Y. Yang, Appl. Phys. Lett. **95**, 013301 (2009).
[23] M. Bokdam, D. Çakır, and G. Brocks, Appl. Phys. Lett. **98**, 113303 (2011).
[24] H. Aarnio, P. Sehati, S. Braun, M. Nyman, M. P. de Jong, M. Fahlman, and R. Österbacka, Adv. Energy Mater. **1**, 792 (2011).
[25] P. Peumans and S. R. Forrest, Chem. Phys. Lett. **398**, 27 (2004).
[26] V. I. Arkhipov, E. V. Emelianova, and H. Bässler, Phys. Rev. Lett. **82**, 1321 (1999).
[27] V. I. Arkhipov, E. V. Emelianova, S. Barth, and H. Bässler, Phys. Rev. B **61**, 8207 (2000).
[28] D. M. Basko and E. M. Conwell, Phys. Rev. B **66**, 155210 (2002).
[29] M. Muntwiler, Q. Yang, W. A. Tisdale, and X.-Y. Zhu, Phys. Rev. Lett. **101**, 196403 (2008).
[30] X.-Y. Zhu, Q. Yang, and M. Muntwiler, Acc. Chem. Res. **42**, 1779 (2009).
[31] H. Ohkita, S. Cook, Y. Astuti, W. Duffy, S. Tierney, W. Zhang, M. Heeney, I. McCulloch, J. Nelson, D. D. C. Bradley, and J. R. Durrant, J. Am. Chem. Soc. **130**, 3030 (2008).
[32] T. M. Clarke, A. M. Ballantyne, J. Nelson, D. D. C. Bradley, and J. R. Durrant, Adv. Funct. Mater. **18**, 4029 (2008).
[33] W. J. Grzegorczyk, T. J. Savenije, T. E. Dykstra, J. Piris, J. M. Schins, and L. D. A. Siebbeles, J. Phys. Chem. C **114**, 5182 (2010).
[34] J. Lee, K. Vandewal, S. R. Yost, M. E. Bahlke, L. Goris, M. A. Baldo, J. V. Manca, and T. V. Voorhis, J. Am. Chem. Soc. **132**, 11878 (2010).
[35] R. D. Pensack and J. B. Asbury, Chem. Phys. Lett. **515**, 197 (2011).
[36] C. Deibel, T. Strobel, and V. Dyakonov, Phys. Rev. Lett. **103**, 036402 (2009).
[37] O. J. Korovyanko, R. Österbacka, X. M. Jiang, Z. V. Vardeny, and R. A. J. Janssen, Phys. Rev. B **64**, 235122 (2001).
[38] J. Guo, H. Ohkita, H. Benten, and S. Ito, J. Am. Chem. Soc. **131**, 16869 (2009).
[39] R. A. Marsh, J. M. Hodgkiss, S. Albert-Seifried, and R. H. Friend, Nano Lett. **10**, 923 (2010).
[40] G. Schönherr, R. Eiermann, H. Bässler, and M. Silver, Chem. Phys. **52**, 287 (1980).
[41] B. Ries and H. Bässler, Phys. Rev. B **35**, 2295 (1987).
[42] R. A. Street, K. W. Song, and J. E. Northrup, Phys. Rev. B **83**, 165207 (2011).

[43]R. A. Street, M. Schoendorf, A. Roy, and J. H. Lee, Phys. Rev. B **81**, 205307 (2010).
[44]T. Kirchartz, B. E. Pieters, J. Kirkpatrick, U. Rau, and J. Nelson, Phys. Rev. B **83**, 115209 (2011).
[45]R. C. I. MacKenzie, T. Kirchartz, G. F. A. Dibb, and J. Nelson, Phys. Chem. C **115**, 9806 (2011).
[46]R. A. Street, S. Cowan, and A. J. Heeger, Phys. Rev. B **82**, 121301(R) (2010).
[47]R. Hesse, W. Hofberger, and H. Bässler, Chem. Phys. **49**, 201 (1980).
[48]M. Scheidler, U. Lemmer, R. Kersting, S. Karg, W. Riess, B. Cleve, R. F. Mahrt, H. Kurz, H. Bässler, E. O. Göbel, and P. Thomas, Phys. Rev. B **54**, 5536 (1996).
[49]A. J. Mozer and N. S. Sariciftci, Chem. Phys. Lett. **389**, 438 (2004).
[50]A. J. Mozer, N. S. Sariciftci, A. Pivrikas, R. Österbacka, G. Juška, L. Brassat, and H. Bässler, Phys. Rev. B **71**, 035214 (2005).
[51]A. M. Ballantyne, L. Chen, J. Dane, T. Hammant, F. M. Braun, M. Heeney, W. Duffy, I. McCulloch, D. D. C. Bradley, and J. Nelson, Adv. Funct. Mater. **18**, 2373 (2008).
[52]R. Mauer, M. Kastler, and F. Laquai, Adv. Funct. Mater. **20**, 2085 (2010).
[53]D. T. Gillespie, J. Comput. Phys. **22**, 403 (1976).
[54]H. Hoppe, N. Arnold, N. S. Sariciftci, and D. Meissner, Sol. Energy. Mater. Sol. Cells **80**, 105 (2003).
[55]P. E. Shaw, A. Ruseckas, and I. D. W. Samuel, Adv. Mater. **20**, 3516 (2008).
[56]T. Förster, Ann. Phys. **437**, 55 (1948).
[57]A. Miller and E. Abrahams, Phys. Rev. **120**, 745 (1960).
[58]M. Casalegno, G. Raos, and R. Po, J. Chem. Phys. **132**, 094705 (2010).
[59]See supplementary material at http://dx.doi.org/10.1063/1.4731698 for additional data.
[60]C. Deibel, D. Mack, J. Gorenflot, A. Schöll, S. Krause, F. Reinert, D. Rauh, and V. Dyakonov, Phys. Rev. B **81**, 085202 (2010).
[61]H. Bässler, Phys. Status Solidi B **175**, 15 (1993).
[62]S. A. Choulis, Y. Kim, J. Nelson, D. D. C. Bradley, M. Giles, M. Shkunov, and I. McCulloch, Appl. Phys. Lett. **85**, 3890 (2004).
[63]H. Yan, S. Swaraj, C. Wang, I. Hwang, N. C. Greenham, C. Groves, H. Ade, and C. R. McNeill, Adv. Funct. Mater. **20**, 4329 (2010).
[64]R. D. Pensack and J. B. Asbury, J. Am. Chem. Soc. **131**, 15986 (2009).
[65]K. Akaike, K. Kanai, H. Yoshida, J. Tsutsumi, T. Nishi, N. Sato, Y. Ouchi, and K. Seki, J. Appl. Phys. **104**, 023710 (2008).
[66]B. P. Rand, D. Burk, and S. R. Forrest, Phys. Rev. B **75**, 115327 (2007).